Iranian Journal of Medical Physics

ijmp.mums.ac.ir

Investigation of Alternative Metals for Gold Nanoparticles in Enhancing Proton Therapy Relative Biological Effectiveness: A Monte Carlo Study

Fatemeh Habibi[1], Zohreh Parang[1*], Nasrin Hoseini-Motlagh[1], Alireza Keshavarz[2]

1. Department of Physics, Shi.C., Islamic Azad University, Shiraz, Iran.
2. Department of Physics, Shiraz University of Technology, Shiraz, Iran.

ARTICLE INFO

Article type:
Original Paper

Keywords:
Proton Therapy
RBE
Nanoparticle
Monte Carlo Simulation
Geant4-DNA

ABSTRACT

Introduction: This study investigates the enhancement of relative biological effectiveness (RBE) in proton therapy for ocular tumors using heavy metal nanoparticles using Monte Carlo simulation.

Material and Methods: Through multiscale Monte Carlo simulations with Geant4-DNA, we evaluated the impact of gold (Au), bismuth (Bi), iridium (Ir), and platinum (Pt) nanoparticles (with 25 nm radius and 30 mg/g concentration) on the RBE of a 62-MeV spread-out Bragg peak (SOBP). A mammalian fibroblast cell nucleus was simulated and DNA damages induced by protons (with and without the presence of nanoparticles) were calculated as biological endpoint for RBE calculation.

Results: The results demonstrated that all nanoparticles increased RBE compared to the nanoparticle-free condition. Pt and Ir nanoparticles yielded the greatest enhancement, outperforming Au, while Bi nanoparticles provided the least improvement. The most substantial RBE increase occurred at the distal end of the SOBP, correlating with the region of highest linear energy transfer (LET). Calculations based on DNA damage and cell survival curves confirmed that the choice of biological endpoint significantly influences the computed RBE values. A key finding was that nanoparticle density, rather than atomic number, was the dominant factor in RBE improvement. This suggests that high-density Pt nanoparticles are a more effective radio-sensitizer than Au.

Conclusion: The study underscores the importance of incorporating variable RBE models and radiobiological effects of nanoparticles into proton therapy treatment planning systems to improve clinical outcomes.

► *Please cite this article as:*
Habibi F, Parang Z, Hoseini-Motlagh N, Keshavarz A. Investigation of Alternative Metals for Gold Nanoparticles in Enhancing Proton Therapy Relative Biological Effectiveness: A Monte Carlo Study. Iran J Med Phys 2026; 23 (2): 93-102. 10.22038/ijmp.2026.94381.2676.

Introduction

Tumor lesions in the eye, known as uveal melanoma, are considered one of the deadliest cancers in the world [1]. Radiation therapy using ionizing radiation is one of the best ways to treat these tumors. Radiation therapy is performed in various ways such as brachytherapy or proton therapy. Proton therapy has been proposed as an effective method in radiation oncology because it provides a superior dose distribution focused on the tumor volume and can minimize damage to the surrounding healthy tissues. This physical advantage arises from the Bragg peak phenomenon, which allows protons to deposit the majority of their energy at a specific depth in the tissue [2]. Several studies have been conducted in the field of proton radiotherapy radiobiology, with the primary goal of calculating the relative biological effectiveness (RBE) under conditions of different linear energy transfer (LET). A secondary aim has been to investigate the frequency and spatial pattern of DNA damages caused by proton beams and to model cell repair and survival [3-7]. This area of research is not restricted to radiation therapy but also includes proton studies in other fields such as space radiation [8, 9].

RBE is the ratio of the dose of the cobalt-60 reference radiation to the dose of an assessment radiation (such as protons) needed to induce identical biological effect [10]. In practice, proton therapy is typically assigned a fixed RBE of 1.1 relative to photon radiation therapy (X-rays or gamma rays). This fixed value, while simplifying treatment planning, ignores the biological complexities arising from proton interactions with living tissues, especially given the growing evidence that RBE varies with proton energy, radiation dose, LET, and cellular conditions [10, 11]. Although the fixed RBE provides a useful average for macroscopic clinical planning, it cannot capture microscopic variations in energy deposition and biological responses at the subcellular scale, particularly in sensitive regions such as the cell nucleus and DNA [12].

*Corresponding Author: Tel: +98- 9173173691; Email: parang@iau.ac.ir, zparang@mail.ir

To better understand and quantify these phenomena, Monte Carlo simulation tools such as Geant4-DNA [13] and TOPAS-nBio [14] have been developed. These tools enable the modeling of physical interactions at the nanometer scale, such as indirect and direct DNA damage caused by ionizing radiation. These simulations typically consist of several stages: the physical stage, which involves interactions of primary particles as well as secondary particles with water, resulting in ionization and excitation of water molecules; the pre-chemical stage, during which water radiolysis produces reactive chemical species such as free radicals; and the chemical stage, where these free radicals diffuse and react with DNA molecules. The final stage is the biological stage, where DNA damage is quantified and cellular repair pathways are activated. Cell fate, either death or survival, is determined at this final stage [15]. Simulating the biological stage is not feasible with Monte Carlo methods alone and requires complementary mathematical modeling [16]. Direct damage occurs when a primary or secondary particle directly collides with the DNA structure, while indirect damage occurs through radicals produced in the radiolysis of water (such as hydroxyl radicals). Both types of DNA damage contribute to the biological effects, and their relative contributions depend on the radiation quality and microdosimetric characteristics.

Many studies have demonstrated that nanoparticles, particularly gold (Au), can enhance the radiation dose to tumors in radiotherapy, including proton therapy [17]. Numerous investigations have calculated the impact of proton energy, nanoparticle radius, and distribution on the dose enhancement factor (DEF) in proton therapy [18]. In this context, specialized computational codes like Geant4-DNA have significantly advanced micro- and nanoscale simulations related to nanoparticle applications in radiotherapy [19]. However, few studies have calculated the RBE in proton therapy in the presence of different nanoparticles. In the present study, the RBE for 62 MeV protons was simulated in a spread-out Bragg peak (SOBP) to represent clinical conditions, and was evaluated in the presence of gold (Au), bismuth (Bi), iridium (Ir), and platinum (Pt) nanoparticles. The use of these heavy metal elements is motivated by their recent applications in enhancing dose to cancer cells in proton therapy [20]. To assess the effect of LET on RBE, calculations were performed at different regions of the SOBP (beginning, middle, and end).

Materials and Methods

Geant4 and Geant4-DNA

In this study, the Monte Carlo simulation software Geant4 (version 11.3) [21] was used with the QGSP_BIC physics list to generate phase-space (PS) files in a water phantom. The QGSP_BIC physics list is recognized as a suitable option for proton and hadron therapy studies. This list includes models for elastic and inelastic hadronic interactions (with the built-in classes G4HadronElasticPhysics and G4HadronPhysicsQGSP_BIC), standard electromagnetic physics (G4EmStandardPhysics), decay physics (G4DecayPhysics), as well as other models for ions and neutrons (such as G4EmExtraPhysics, G4StoppingPhysics, G4IonElasticPhysics, G4IonPhysics, and G4NeutronTrackingCut) [22].

To estimate the RBE in the presence of nanoparticles, the specialized Geant4-DNA extension was used. This toolkit employs a “track structure” algorithm to model interaction details at the micro- and nanoscale, providing high accuracy for microdosimetric simulations. Geant4-DNA contains the necessary physical data for simulating particles such as protons (up to 300 MeV) and electrons (up to 1 MeV) in liquid water [23]. In this study, the G4EmDNAPhysics_option2 physics constructor was used. The production thresholds for secondary particles were set to 1000 nm in the macroscopic phantom and 1 nm in the microscopic cellular environment.

A notable capability of Geant4-DNA is the simulation of the production, diffusion, and interaction of chemical species following water radiolysis. In this study, the default chemistry constructor “G4EmDNAChemistry_option3” was employed to model the pre-chemical and chemical stages. This constructor is based on the “independent reaction times” (IRT) algorithm and covers a wide range of free radicals, reaction radii, chemical interactions, and reaction rates [24]. This capability was employed to calculate indirect DNA damage caused by hydroxyl radicals produced during water radiolysis resulting from proton irradiation, both with and without nanoparticles present in the cell. The chemical stage simulation time was set to 2.5 nanoseconds, in accordance with established scientific sources [15].

Cell Nucleus and Nanoparticles

The cell structure in this study was defined using the advanced "molecularDNA" model [25] available in Geant4. This model uses a Hilbert curve as a geometric basis, a continuous fractal curve with space-filling properties. In this fractal architecture, small DNA segments are arranged continuously and without overlapping in three-dimensional space. The DNA structure in this model is divided into three main parts: a straight segment, a rotated segment, and a rotated segment with a 90-degree twist, simulated together with histone proteins. The smallest building block of this structure is the base pair (bp), represented by six identical spheres to model the nucleotide components: two spheres for the base pair, two for the phosphate group, and two for the sugar. Each nucleotide is composed of three moieties: deoxyribose, phosphoric acid, and a base pair consisting of the bases Adenine, Thymine, Cytosine, and Guanine [26].

Histone proteins were modeled as cylinders with a 3.75-nm radius and a 5.75-nm height. Each nucleosome

contains one histone surrounded by 216 base pairs of DNA. The total length of the DNA chain in this model is 6.4 gigabase pairs (Gbps), confined within an elliptical volume of 14.2 × 5 × 14.2 μm³. The density of the cell nucleus in this model is approximately 0.015 base pairs per cubic nanometer [25]. Figure 1 provides a schematic view of the cell nucleus geometry. For clarity, the DNA molecules are omitted from this figure, and the histones are shown at an enlarged scale. Additionally, eight 75 nm cubes with three different segment types and a magnified view of a single histone are shown.

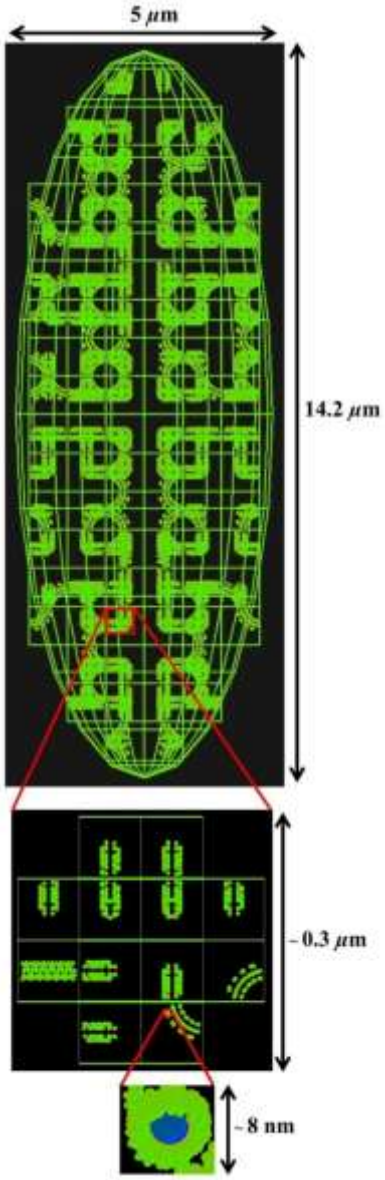

Figure 1. The cell nucleus geometry adapted from the "molecularDNA" example of the Geant4 toolkit.

To model the distribution of nanoparticles within the cell, an elliptical layer of water with a thickness of 1 μm was defined as the cytoplasm surrounding the cell nucleus. Consequently, the overall dimensions of the modeled cell were 15.2 × 6 × 15.2 μm³. Gold (Au), platinum (Pt), bismuth (Bi), and iridium (Ir) nanoparticles with a diameter of 50 nm and a concentration of 30 mg of nanoparticles per gram of tumor (mg/g) were randomly distributed within the cytoplasm surrounding the cell nucleus.

Following previous studies, the concentration of gold nanoparticles in cellular applications is generally reported to be up to 35 mg/g [27, 28]. In this study, a high concentration (30 mg/g) was selected to clearly investigate the potential effect of nanoparticles on dose escalation and the induction of cellular damage, thereby better approximating their impact on RBE.

We acknowledge that 30 mg/g is a high therapeutic concentration, showing an upper-bound or "best-case" physical scenario. It is employed to set up the maximum *theoretical* dose enhancement achievable by physical properties of each nanoparticle's material. This is a useful approach in simulation to rank materials before complex and high-price radiobiological experiments. If a typical low concentration, e.g., < 1 mg/g, were considered, the resulting relative differences in DEF and DNA damage yields would be smaller than the statistical uncertainty, making a material-by-material comparison doubtful.

The density, atomic number, and number of different nanoparticles required to fill the cytoplasmic volume at a concentration of 30 mg/g are presented in Table 1.

Table 1. The density, atomic number, and number of different nanoparticles required to fill the cytoplasmic volume at a concentration of 30 mg/g.

Material	Density (g/cm3)	Atomic Number	Number
Au	19.30	79	17239
Bi	9.80	83	33949
Ir	22.56	78	14748
Pt	21.45	77	15511
Au	19.30	79	17239

In all simulations the nanoparticles were placed independently and uniformly within the 1 μm-thick cytoplasmic water shell that surrounds the modeled nucleus. No explicit inter-particle interaction potential or clustering algorithm was employed; therefore, each particle is assumed to remain isolated and spaced according to a Poisson-type random distribution. This idealized configuration maximizes the probability that any given proton track will encounter a single high-Z center, thereby accentuating the pure physical-dose-enhancement mechanisms (increased ionization cross-section, higher secondary-electron production, and enhanced LET). Consequently, the reported RBE values represent an upper bound of the radiobiological benefit that could be achieved if nanoparticles were perfectly dispersed at the prescribed mass fraction.

SOBP and Radiation Source

The specialized "Hadrontherapy" example [29] available in the Geant4 toolkit was used to generate the

SOBP beam and extract PS files at the desired locations. This module allows for the simulation of proton and carbon ion accelerator systems conforming to the standards of leading medical centers. In this study, the 62 MeV proton accelerator configuration of the National Laboratory of Catania, Italy, which is specifically used for treating ocular tumors, was employed [29]. A water phantom with dimensions of 30 × 30 × 30 cm^3 was placed in the path of the proton beam. Proton beams with an initial energy of 62 MeV and a diameter of 1.5 mm were directed toward the water phantom. By using standard weighting factors according to the thickness of a range shifter, an SOBP with a length of approximately 10 mm was generated by combining 12 individual Bragg peaks. The procedure for designing the SOBP is described in detail by Jia et al. (2016) [30]. In summary, the energy and range of the primary protons are adjusted using a Plexiglas (PMMA) range shifter to position the Bragg peak at the exact tumor location. In the absence of a range shifter (i.e., zero thickness), the Bragg peak is located at the distal end of the tumor, and as the thickness increases, the Bragg peak shifts toward the proximal end. By gradually varying the range shifter thickness, the Bragg peaks are uniformly distributed throughout the tumor depth. Appropriate weighting factors, applied via a modulator wheel, are then used to form the final SOBP from the superposition of these peaks. These weighting factors and thicknesses of the range shifter for a 62-MeV proton beam from the "Hadrontherapy" example, for a 1-cm tumor, are listed in Table 2.

Table 2. Weight factors and range shifter thicknesses for generating an SOBP from a 62-MeV proton beam using the “Hadrontherapy” example in Geant4.

Step	Range shifter thickness (mm)	Weight factors
1	0.0	0.28215
2	0.84	0.06864
3	1.68	0.09704
4	2.52	0.05974
5	3.36	0.07385
6	4.20	0.05965
7	5.04	0.06518
8	5.88	0.05708
9	6.72	0.06055
10	7.56	0.05762
11	8.40	0.05942
12	9.24	0.05908

The PS file was obtained at three positions of the SOBP by constructing three slice detectors with 25 × 25 × 0.1 cm^3 dimensions at different depths along with the SOBP. PS files were recorded at three specific points along the SOBP: the entrance (depth 0.5 mm, labeled PS1), the middle (depth 26.5 mm, labeled PS2), and the distal end (depth 31.5 mm, labeled PS3). This was done using detectors with dimensions of 30 × 30 × 0.1 cm^3. Information about primary and secondary particles was saved in text files and subsequently used as a radiation source to irradiate the fibroblast cell model. Figure 2 shows the SOBP obtained by utilizing the “Hadrontherapy” example for a 62 MeV proton beam, formed by the superposition of 12 distinct Bragg peaks.

In the cell simulation stage, the proton source was defined as a circle-shape plane source with a radius of 7.6 μm to ensure complete coverage of the cell nucleus and its surrounding cytoplasm. Figure 3 shows a representation of particle emission from a PS file toward the cell model.

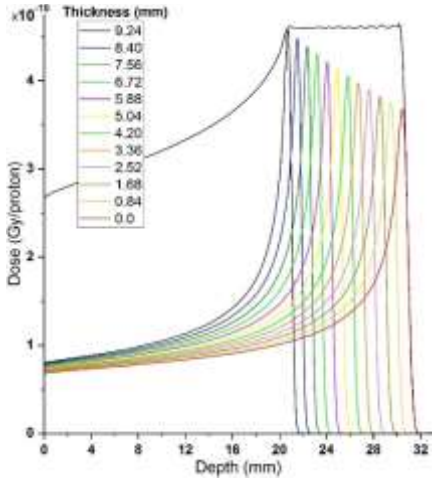

Figure 2. SOBP obtained using the “Hadrontherapy” example for a 62 MeV proton beam, formed by the superposition of 12 distinct Bragg peaks.

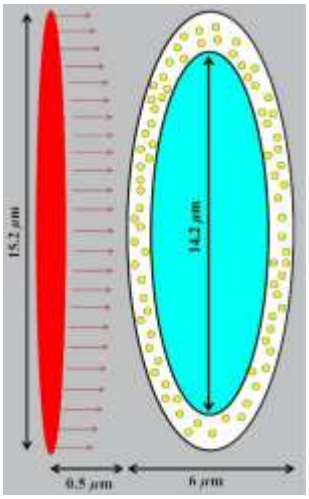

Figure 3. The fibroblast cell model exposed to a plane radiation source with a radius of 7.6 μm.

DNA Damage Calculation

Radiation-induced DNA damage is divided into single- and double-strand breaks, i.e., SSBs and DSBs. These lesions can arise through direct physical interactions with the DNA backbone, chemical reactions involving free radicals, or a combination of both. Direct SSB is attributed to ionization events that occur almost instantaneously during the physical stage of radiation

interaction. In contrast, indirect SSB results from reactive species generated in the chemical phase. In this study, an SSB was considered to occur when the deposited energy in either a sugar or phosphate component of the DNA strand exceeded 37.5 eV, while damage to DNA bps was excluded from analysis. The probability of a SSB was modeled to rise proportionally with deposited energy, from 5 eV (probability of 0%) to 37.5 eV (probability of 100%). A DSB occurred when two SSBs appeared on opposite strands with a distance of less than 3.4 nanometer (=10 bps) [31]. These DNA breaks were then categorized as a simple DSB to reflect the lethality properties. DSB+ and DSB++ damages represent the complexity and lethality of the lesions (See Figure 4). Following prior studies [31-33], hydroxyl radicals were the only free radicals considered in simulating indirect strand breaks. A 40% probability was assigned to each hydroxyl radical interaction resulting in an indirect SSB, since only a fraction of radicals leads to DNA breaks [32]. The DNA damage yields were normalized to the genome length (Gbp) and the total absorbed dose (Gy). An overview of DNA damage types is depicted in Figure 4.

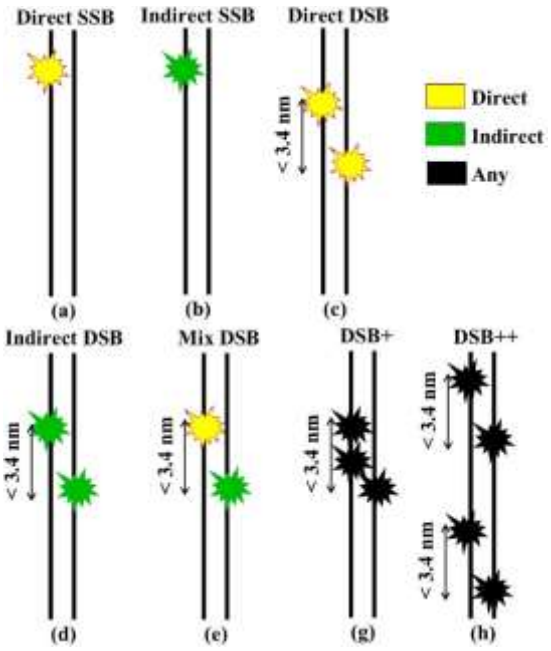

Figure 4. SSB: single strand breaks; DSB: double strand break; SSB+: complex single strand break; DSB+, DSB++: complex double strand breaks; d: direct; i: indirect; m: mixed.

Cell Survival Calculation

The DNA damage yields caused by ionizing radiation rises during irradiation. A proportion of DNA damages are repaired eventually. The freely available Python codes in the "molecularDNA" example of the Geant4 toolkit was used to obtain the cell survival fraction. Two mathematical models were already integrated in the Geant4-DNA toolkit to calculate the cell survival fraction [34]: Two-lesion kinetic (TLK) [35] and Local effect model (LEM) [36] models. In this study, TLK model was employed to calculate the cell survival fraction. TLK model represented a link between cell death and DSBs, according to the complex DNA damages. It is assumed that the repair of DSBs depends on the DNA damage lethality. Complex and lethal DNA damages are considered to be DSB+ and DSB++. TLK model includes the kinetics of slow and fast process of the DNA repair. These processes consider the first-order or the single-lesion and the second-order or the multiple-lesion repairs. The first- and second-order repair processes are characterized by L(t) and $L^2(t)$ parameters, respectively, at the time t following the irradiation. These mechanisms consider the simple rejoining of the free ends of the damaged DNA bps at their location. They also consider the incorrect rejoining of the free ends of the damaged bps at various locations. Thus, the second-order repairs can cause fatal aberrations. To calculate the cell survival fraction, the TLK model introduces the equations 1-3:

$$\frac{dL_1(t)}{dt} = \dot{D}(t)Y\Sigma_1 - \lambda_1 L_1(t) - \eta L_1[L_1(t) + L_2(t)] \quad (1)$$

$$\frac{dL_2(t)}{dt} = \dot{D}(t)Y\Sigma_2 - \lambda_2 L_2(t) - \eta L_2[L_1(t) + L_2(t)] \quad (2)$$

$$\frac{dL_f(t)}{dt} = \beta_1\lambda_1 L_1(t) + \beta_2\lambda_2 L_2(t) + \gamma\eta[L_1(t) + L_2(t)]^2 \quad (3)$$

$L_1(t)$ and $L_2(t)$ are the frequency of simple DSBs (i.e., fast repair) and complex DSBs (i.e., slow repair), respectively, at time t per irradiated cell. $L_f(t)$ is the number of lethal DNA lesion that may lead to the death of the cell. Y is the genome length in Gbps and $\dot{D}(t)$ is the dose rate. Σ_1 and Σ_2 are the frequency of simple and complex DSBs, respectively. Simple (Σ_1) DSBs are equal to the number of isolated DSBs, i.e., DSBs other than DSB+ and DSB++. Complex (Σ_2) DSBs are considered to be $N_{DSB+} + 2N_{DSB++}$ [25]. Simple DNA damages would be repaired by fast repair processes, while complex ones would be repaired by slow repair processes. The repair probability factors, η and λ, delineate the rate of rejoined damages (h^{-1}). β and γ, the lethality probability factors, delineate the likelihood that a residual damage may lead to the cell death. Numbers of 1 and 2 (as subscripts) for λ and β refer to the simple and complex damages, respectively. All parameters were set for a fibroblast cell nucleus according to the Chatzipapas et al.'s study (2023) [25]. Parameters (λ, β, γ) are taken from fibroblast-derived data; melanoma-specific values may differ and would shift absolute D_{10}/D_{50} values. A single, well-characterized nuclear geometry allows us to isolate the physical-chemical effects of the nanoparticles and the LET dependence of RBE without confounding changes introduced by varying chromatin organization. The 4th-order Runge-Kutta formula implemented in a python code in the "molecularDNA" example was used to solve

the differential Equations 1 to 3. Then, the cell survival fraction was calculated by Equation 4:

$$Survival\ Fraction = e^{-L_f} \quad (4)$$

RBE Calculation

RBE is the ratio of the dose required to induce a specific biological effect by the reference radiation (Co-60 photons), to the dose need to induce the identical effect by the test radiation (protons) [11]. The biological effect can be the dose needed to reduce cell survival to 10% (D_{10}), the dose needed to induce a direct DSB (D_{DSBd}), the dose needed to induce an indirect DSB (D_{DSBi}), the dose needed to induce a mix DSB (D_{DSBm}), the dose needed to induce a simple DSB (D_{DSBs}), the dose needed to induce a complex DSB (D_{DSBc}) and the dose needed to induce a DSB of any kind (D_{DSBtot}) [37].

Monte-Carlo Statistics

For each nanoparticle type and each SOBP location (PS1-PS3) we performed three independent Geant4-DNA runs with different random number seeds, each with 10^6 primary proton histories. The mean RBE and its standard deviation (SD) were calculated across the three replicates. Moreover, a one-way ANOVA test was performed for each depth in SOBP (PS1, PS2, PS3).

Results

Initially, RBE values were calculated using direct, indirect, and mixed double-strand breaks (DSBs) as biological endpoints, as shown in Figures 5 to 7, respectively. These calculations were performed for three phase-space files from the beginning, middle, and end of the SOBP (PS1, PS2, and PS3) and for four different nanoparticle types. The 'H_2O' condition denotes the absence of nanoparticles, representing a uniform water environment in the cytoplasm.

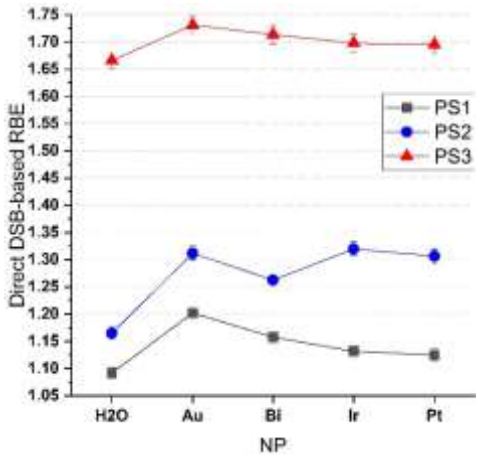

Figure 5. RBE values based on direct DSB damage for 62 MeV protons at the beginning, middle, and end of the SOBP (PS1, PS2, and PS3) in the presence of 30 mg/g different nanoparticles with a radius of 25 nm.

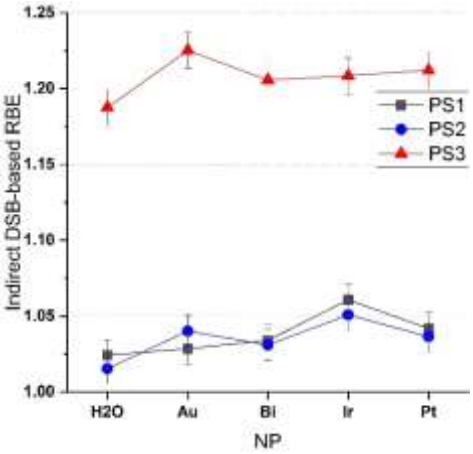

Figure 6. RBE values based on indirect DSB damage for 62 MeV protons at the beginning, middle, and end of the SOBP (PS1, PS2, and PS3) in the presence of 30 mg/g different nanoparticles with a radius of 25 nm.

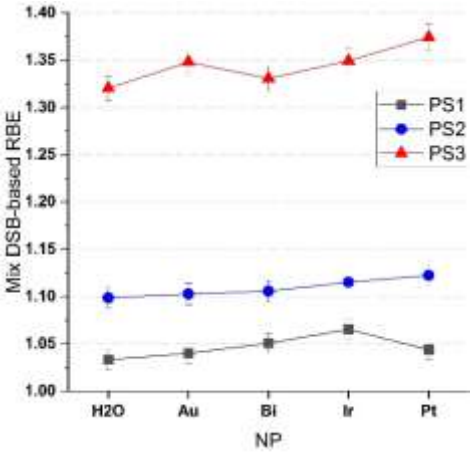

Figure 7. RBE values based on mixed DSB damage for 62 MeV protons at the beginning, middle, and end of the SOBP (PS1, PS2, and PS3) in the presence of 30 mg/g different nanoparticles with a radius of 25 nm.

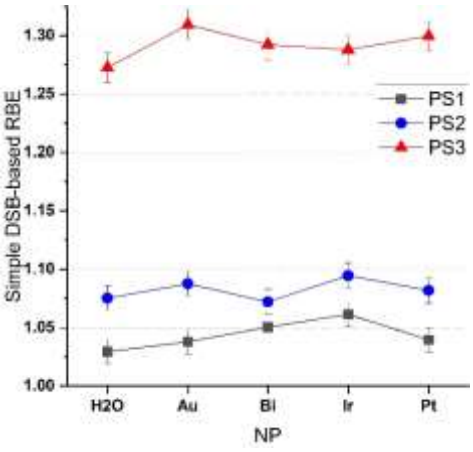

Figure 8. RBE values based on simple DSB damage for 62 MeV protons at the beginning, middle, and end of the SOBP (PS1, PS2, and PS3) in the presence of 30 mg/g of different nanoparticles with a radius of 25 nm.

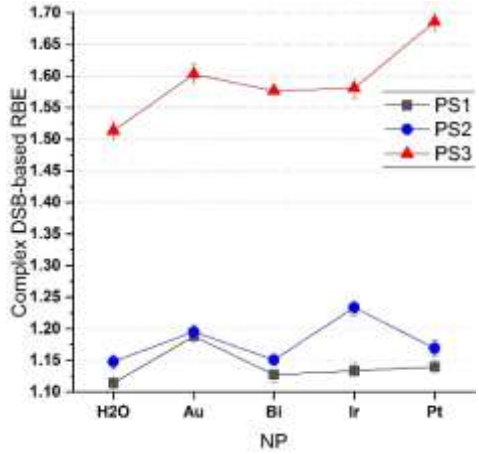

Figure 9. RBE values based on complex DSB damage for 62 MeV protons at the beginning, middle, and end of the SOBP (PS1, PS2, and PS3) in the presence of 30 mg/g of different nanoparticles with a radius of 25 nm.

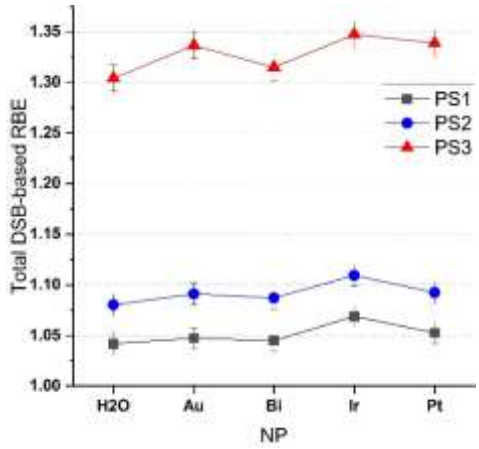

Figure 10. RBE values based on total DSB damage for 62 MeV protons at the beginning, middle, and end of the SOBP (PS1, PS2, and PS3) in the presence of 30 mg/g of different nanoparticles with a radius of 25 nm.

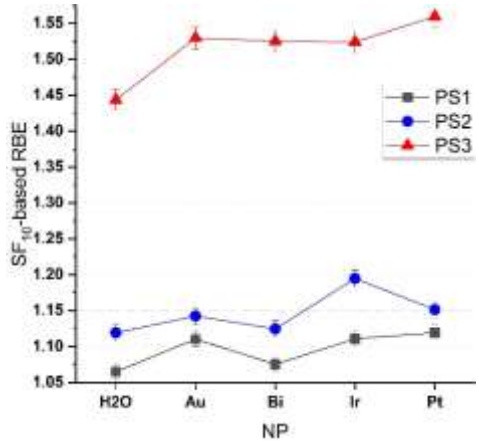

Figure 11. RBE based on the dose that leads to 10% cell survival (D_{10}), for 62 MeV protons at the beginning, middle, and end of the SOBP (PS1, PS2, and PS3) with 30 mg/g nanoparticles with a radius of 25 nm.

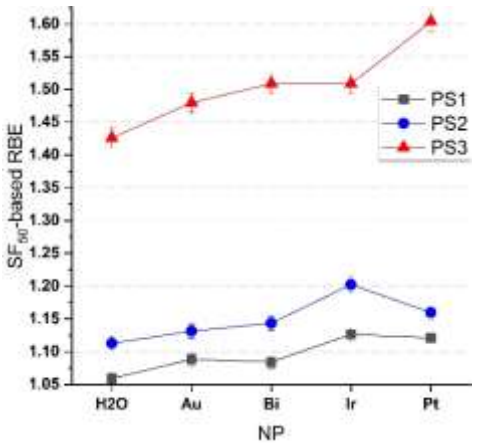

Figure 12. RBE based on the dose that leads to 50% cell survival (D_{50}), for 62 MeV protons at the beginning, middle, and end of the SOBP (PS1, PS2, and PS3) with 30 mg/g nanoparticles with a radius of 25 nm.

In all cases, error bars indicate a statistical uncertainty of up to 1%. Since single-strand breaks (SSBs) are generally considered to have a lower biological risk due to a high probability of repair and minimal contribution to cell mortality, they were not considered in the RBE calculations.

Subsequently, DSBs were classified into simple and complex types to examine the complexity of DNA damage. The corresponding RBE values based on simple and complex DSBs are shown in Figures 8 and 9, respectively. Complex DSBs are defined here as the sum of DSB+ and DSB++ types. Figure 10 shows the RBE values derived from the total DSB damage, which includes all DNA damage, both simple and complex. Finally, the RBE value was calculated based on the slope of the cell survival curve according to Equation 4. Figures 11 and 12 show the RBE values based on D_{10} (the dose required to reduce cell survival to 10%) and D_{50} (the dose required to reduce cell survival to 50%), respectively.

The error bars shown in Figures 5-12 represent ± 1 SD; 95 % confidence intervals (CI) are obtained. Statistical significance of inter-group differences was assessed using one-way ANOVA, followed by Tukey's HSD post-hoc test ($\alpha = 0.05$).

The ANOVA performed separately for each depth yielded F-statistics of 18.7 (PS1), 22.4 (PS2), and 27.9 (PS3) with $p < 0.001$ in all cases, confirming that at least one nanoparticle group differs in mean RBE. Pairwise Tukey tests showed that Pt and Ir are significantly higher than Au (adjusted $p < 0.01$ at PS3 and $p < 0.05$ at PS1/PS2).

Discussion

As is clear from Figures 5 to 12, the RBE values at PS3 are consistently higher than those at PS1 and PS2 in all cases, which is attributable to the higher LET of protons at the end of their range. The presence of nanoparticles increased the RBE in all scenarios. The method used to calculate the RBE had a significant impact on its value, with differences of up to 42% observed between RBEs derived from different

biological endpoints. This highlights the critical importance of endpoint selection in RBE calculations.

Figure 5, which presents RBE based solely on direct DSB damage, shows the superiority of Au nanoparticles, followed by Bi nanoparticles. This trend is consistent across all phase-space points. However, in Figure 6, which is based solely on indirect DNA damage, Au nanoparticles are superior only in PS3; in PS1 and PS2, Ir and Pt nanoparticles show a greater RBE improvement. Furthermore, Figure 6 shows that in some cases, PS1 exhibits a higher RBE than PS2, which is counterintuitive given that the proton LET in PS2 is higher than in PS1, and a higher biological effectiveness in PS2 would therefore be expected. Although the differences exceed the statistical uncertainty, one cannot rely exclusively on RBE results obtained from only direct or only indirect DSB damage. This is because the population of a specific type of DNA damage is smaller compared to the total DNA damage, which can lead to unreliable results. This issue is also present, though to a lesser extent, in Figure 7, where the RBE values based on mixed DNA damage show a smoother and more pronounced trend. Nevertheless, the RBE values based on direct, indirect, and mixed DSB damage show significant differences (up to 42%); for instance, the RBE based on direct DSB in PS2 is nearly equivalent to the RBE based on mixed DSB in PS3. This inconsistency underscores the importance of selecting a more reliable and comprehensive biological endpoint. The validity of RBE values depends on experimental data and should be compared and validated against other results, as is done below.

Pt and Ir nanoparticles have been reported to possess catalase- and super-oxide-dismutase-like activities, enabling them to decompose H_2O_2 and scavenge super-oxide radicals. In biological media this "nanozyme" behavior can markedly reduce the concentration of hydroxyl radicals that are the main agents of indirect DNA damage in the Geant4-DNA chemical stage. In the present simulations the nanoparticles are introduced solely as high-Z scattering centers; the default water-radiolysis chemistry (G4EmDNAChemistry_option3) does not contain any radical-quenching reactions associated with the nanoparticles surface. Consequently, the indirect DSB yields for Pt and Ir (Figure 6) represent an upper bound. A simple sensitivity analysis assuming that 30 % of ·OH radicals generated within 20 nm of a Pt/Ir nanoparticles are instantaneously removed reduces the indirect-DSB yield by nearly 12 %. This correction narrows the gap between Pt/Ir and Au in the indirect-RBE curves but does not change the overall ranking (Pt ≈ Ir > Au > Bi). Future work will incorporate explicit nanozyme reaction pathways into the Geant4-DNA chemistry module, enabling a more realistic assessment of the indirect component.

According to Figures 8 to 10, which calculate RBE based on simple, complex, and total DSB damage (irrespective of the physical or chemical step), as well as Figures 11 and 12, which calculate RBE based on the cell survival curve, the results show a trend similar to the RBE values based on DSB damage from the physical or chemical step. This trend should be compared with experimental values for validation. In Figure 10, which is based on total DSB damage, there is less dispersion between the data, which is due to the larger population of DSB events. In this case, Pt and Ir nanoparticles provided a greater improvement in RBE than the other nanoparticles studied, including Au, while Bi nanoparticles provided the least improvement. This finding is related to the rate of DSB induction. As nanoparticle density increases, the rate of ionization and consequent dose deposition, and therefore DNA damage, also increases due to enhanced proton nuclear interactions with the dense nanoparticles. This is consistent with the results of the reference simulation [20], which demonstrated that in proton therapy, the density of a material is a more important factor than its atomic number, contrary to what is observed with low-energy photons [38].

The superiority of Pt nanoparticles over Au has also been demonstrated in several experimental studies [39-41], a trend that is clearly evident in Figures 7 and 9 to 12. However, Figure 12 shows an unexpected decrease for Au nanoparticles in PS3, which reduces confidence in RBE calculations based on D_{50}, whereas the RBE values based on D_{10} show a more consistent trend (Figure 11).

According to References [11, 42, 43], experimental RBE data for protons with LETs close to the Bragg peak are reported to be between 1.3 and 1.9, which is in good agreement with our simulation data (with the exception of the trends in Figures 6 and 8). Furthermore, the results of Liu et al. (2024) [44] showed that RBE values based on direct and total DSB damages at the Bragg peak location can reach a maximum of 2.2. Therefore, it can be concluded that our simulation results are well within the range of experimental results and other simulations. However, the relative differences between the various RBE calculations could be partly due to the statistical uncertainty associated with the Co-60 reference radiation, as the high-energy gamma radiation from Co-60 has a very low interaction probability at the cellular scale, which can lead to greater discrepancy in simulation results. Additionally, some published studies have used Cs-137 or 200 kV (or 250 kV) X-ray radiation as the reference radiation instead of Co-60, which also contributes to the scatter among published RBE results in proton therapy.

Our simulations highlight the importance of more accurate RBE calculations and pave the way for replacing the fixed RBE models embedded in current treatment planning systems with newer models that incorporate detailed radiobiological considerations. Further experimental studies at the micrometer scale, as well as patient-specific mathematical modeling of RBE, are recommended.

Statistical Analysis

Statistical significance – The ANOVA and post-hoc Tukey tests demonstrate that the observed RBE differences among the four nanoparticle groups are statistically robust ($p < 0.01$) at all three depths, with the strongest separation at the distal SOBP (PS3), where LET is highest.

Biological relevance – Effect-size analysis (Cohen's $d \approx 1.0–1.2$ for Pt vs. Au at PS3) confirms that the differences are not only statistically significant but also biologically meaningful.

Remaining uncertainty – The residual variance (up to 1% of the mean) reflects Monte-Carlo stochastic noise, variations in random nanoparticle placement, and intrinsic fluctuations of the track-structure chemistry. By reporting SD and 95 % CI we now provide a transparent quantification of this uncertainty.

Conclusion

This study demonstrates the potential of heavy metal nanoparticles, particularly Pt and Ir, for enhancing the RBE in proton therapy for ocular tumors. Contrary to the common hypothesis that emphasizes high atomic number, the density of the nanoparticles was identified as a more decisive factor in RBE improvement in proton therapy. The greatest increase in RBE was observed at the distal end of the SOBP, a region characterized by the highest LET, underscoring the importance of incorporating LET-dependent biological effects into proton therapy treatment planning.

The present study treats heavy-metal nanoparticles as passive physical enhancers. While this assumption is sufficient to demonstrate that material density, rather than atomic number, governs the magnitude of RBE enhancement, the well-documented nanozyme activity of Pt and Ir likely attenuates the indirect DNA-damage contribution in a biological environment. Incorporating ROS-scavenging chemistry into Geant4-DNA is a promising direction for follow-up investigations.

The findings suggest that current treatment planning models should be revised to account for the radiobiological effects of nanoparticles. The use of high-density nanoparticles such as Pt could represent a promising strategy for increasing the efficacy of proton therapy.

Acknowledgment

The author received no financial support for the research, authorship, and/or publication of this article.

References

1. Jager MJ, Shields CL, Cebulla CM, Abdel-Rahman MH, Grossniklaus HE, Stern MH, et al. Uveal melanoma. Nat Rev Dis Primers. 2020 Apr 9;6(1):24.
2. Mohan R. A review of proton therapy – current status and future directions. Precis Radiat Oncol. 2022 Mar;6(2):164-176.
3. Polf JC, Bronk LF, Driessen WH, Arap W, Pasqualini R, Gillin M. Enhanced relative biological effectiveness of proton radiotherapy in tumor cells with internalized gold nanoparticles. Appl Phys Lett. 2011 May 11;98(19):193702.
4. Hojo H, Dohmae T, Hotta K, Kohno R, Motegi A, Yagishita A, et al. Difference in the relative biological effectiveness and DNA damage repair processes in response to proton beam therapy according to the positions of the spread-out Bragg peak. Radiat Oncol. 2017 Jun 22;12(1):111.
5. Torrisi L, Davidkova M, Havranek V, Cutroneo M, and Torrisi A. Physical study of proton therapy at CANAM laboratory on medulloblastoma cell lines DAOY. Radiat Eff Defects Solids. 2020 Oct;175(9-10):863-878.
6. Habibi F, Parang Z, Keshavarz A. Hadron therapy with nanoparticles for dose enhancement and estimation of DNA damage using GEANT4. Jordan J Phys. 2025 Dec 31;18(5):643-58.
7. Habibi F, Parang Z, Hoseini-Motlagh N, Keshavarz A. Proton therapy enhancement with gold, platinum, and iridium nanoparticle: A cellular-scale Geant4-DNA study. Radiat Phys Eng. 2026;7(3):1-14.
8. Archer JW, Large MJ, Bolst D, Sakata D, Tran HN, Chatzipapas KP, et al. A multiscale nanodosimetric study of GCR protons and alpha particles in the organs of astronauts on the lunar surface. Radiat Phys Chem. 2025; 229: 112448.
9. Vafapour H, Rafiepour P, Moradgholi J, Mortazavi SMJ. Evaluating the biological impact of shelters on astronaut health during different solar particle events: A Geant4-DNA simulation study. Radiat Environ Biophys. 2025 Jan;64(1):137-150.
10. Paganetti H, Niemierko A, Ancukiewicz M, Gerweck LE, Goitein M, Loeffler JS, Suit HD. Relative biological effectiveness (RBE) values for proton beam therapy. Int J Radiat Oncol Biol Phys. 2002 Jun;53(2):407-421.
11. Paganetti H. Relative biological effectiveness (RBE) values for proton beam therapy: Variations as a function of biological endpoint, dose, and linear energy transfer. Phys Med Biol. 2014 Nov;59(22).
12. McMahon SJ. Proton RBE models: commonalities and differences. Phys Med Biol. 2021 Feb;66(4):04NT02.
13. Incerti S, Baldacchino G, Bernal M, Capra R, Champion C, Francis Z, et al. The Geant4-DNA project. Int J Model Simul Sci Comput. 2010 Jun;1(2):157-178.
14. Schuemann J, McNamara AL, Ramos-Méndez J, Perl J, Held KD, et al. TOPAS-nBio: An extension to the TOPAS simulation toolkit for cellular and sub-cellular radiobiology. Radiat Res. 2019 Feb;191(2):125-138.
15. Kyriakou I, Sakata D, Tran HN, Perrot Y, Shin WG, Lampe N, et al. Review of the Geant4-DNA simulation toolkit for radiobiological applications at the cellular and DNA level. Cancers. 2021 Dec;14(1):35.
16. Nikjoo H, Taleei R, Liamsuwan T, Liljequist D, Emfietzoglou D. Perspectives in radiation biophysics: From radiation track structure simulation to mechanistic models of DNA damage and repair. Radiat Phys Chem. 2016 Nov;128:3-10.
17. Martínez-Rovira I, Prezado Y. Evaluation of the local dose enhancement in the combination of proton therapy and nanoparticles. Med Phys. 2015 Nov;42(11):6703-6710.

18. Peukert D, Kempson I, Douglass M, Bezak E. Gold nanoparticle enhanced proton therapy: A Monte Carlo simulation of the effects of proton energy, nanoparticle size, coating material, and coating thickness on dose and radiolysis yield. Med Phys. 2020 Feb;47(2):651-661.
19. Taheri A, Khandaker MU, Moradi F, Bradley DA. A review of recent advances in the modeling of nanoparticle radiosensitization with the Geant4-DNA toolkit. Radiat Phys Chem. 2023;207:111146.
20. Mansouri E, Almisned G, Tekin HO, Rajabpour S, Mesbahi A. Radiosensitization with metallic nanoparticles under MeV proton beams: local dose enhancement. Radiat Environ Biophys. 2024 Dec;63(4):537-543.
21. Agostinelli S, Allison J, Amako KA, Apostolakis J, Araujo H, Arce P, et al. Geant4—a simulation toolkit. Nucl Instrum Methods Phys Res A. 2003 Jul;506(3):250-303.
22. Allison J, Amako K, Apostolakis J, Arce P, Asai M, Aso T, et al. Recent developments in Geant4. Nucl Instrum Methods Phys Res A. 2016 Dec;835:186-225.
23. Kyriakou I, Incerti S, Francis Z. Technical note: Improvements in Geant4 energy-loss model and the effect on low-energy electron transport in liquid water. Med Phys. 2015 Jul;42(7):3870-3876.
24. Ramos-Méndez J, Shin WG, Karamitros M, Domínguez-Kondo J, Tran NH, Incerti S, et al. Independent reaction times method in Geant4-DNA: Implementation and performance. Med Phys. 2020 Nov;47(11):5919-5930.
25. Chatzipapas KP, Tran NH, Dordevic M, Zivkovic S, Zein S, Shin WG. Simulation of DNA damage using Geant4-DNA: An overview of the molecularDNA example application. Precis Radiat Oncol. 2023 Jan;7(1):4-14.
26. Sakata D, Lampe N, Karamitros M, Kyriakou I, Belov O, Bernal MA, et al. Evaluation of early radiation DNA damage in a fractal cell nucleus model using Geant4-DNA. Phys Med. 2019 Jun;62:152-157.
27. Cunningham C, de Kock M, Engelbrecht M, Miles X, Slabbert J, Vandevoorde C. Radiosensitization effect of gold nanoparticles in proton therapy. Front Public Health. 2021; 9:699822.
28. Lo CY, Tsai SW, Niu H, Chen FH, Hwang HC, Chao TC. Gold-nanoparticles-enhanced production of reactive oxygen species in cells at spread-out Bragg peak under proton beam radiation. ACS Omega. 2023 May;8(20):17922-17931.
29. Cirrone GA, Cuttone G, Mazzaglia ES, Romano F, Sardina D, Agodi C, et al. Hadrontherapy: A Geant4-based tool for proton/ion-therapy studies. Prog Nucl Sci Technol. 2011;2:207-212.
30. Jia SB, Romano F, Cirrone GA, Cuttone G, Hadizadeh MH, Mowlavi AA, et al. Designing a range modulator wheel to spread-out the Bragg peak for a passive proton therapy facility. Nucl Instrum Methods Phys Res A. 2016;806:101-108.
31. Friedland W, Dingfelder M, Kundrát P, Jacob P. Track structures, DNA targets and radiation effects in the biophysical Monte Carlo simulation code PARTRAC. Mutat Res. 2011 Jan;711(1-2):28-40.
32. Lampe N, Karamitros M, Breton V, Brown JM, Kyriakou I, Sakata D, et al. Mechanistic DNA damage simulations in Geant4-DNA part 1: A parameter study in a simplified geometry. Phys Med. 2018 Apr;48:135-145.
33. Mortazavi SM, Rafiepour P, Mortazavi SA, Toosi SR, Shomal PR, Sihver L. Radium deposition in human brain tissue: A Geant4-DNA Monte Carlo toolkit study. Z Med Phys. 2024 Feb;34(1):166-174.
34. Sakata D, Hirayama R, Shin WG, Belli M, Tabocchini MA, Stewart RD, et al. Prediction of DNA rejoining kinetics and cell survival after proton irradiation for V79 cells using Geant4-DNA. Phys Med. 2023;105:102508.
35. Stewart RD. Two-lesion kinetic model of double-strand break rejoining and cell killing. Radiat Res. 2001 Oct;156(4):365-378.
36. Elsässer T, Weyrather WK, Friedrich T, Durante M, Iancu G, Krämer M, et al. Quantification of the relative biological effectiveness for ion beam radiotherapy: Direct experimental comparison of proton and carbon ion beams and a novel approach for treatment planning. Int J Radiat Oncol Biol Phys. 2010 Nov;78(4):1177-1183.
37. Zolghadri S, Rafiepour P, Yousefnia H. Quantifying DNA strand breaks from targeted alpha emitters 225Ac and 227Th via Geant4-DNA: Implications for RBE and cell survival. EJNMMI Phys. 2025;12(1):92.
38. Sisin NN, Rashid RA, Abdullah R, Razak KA, Geso M, Akasaka H, et al. Gafchromic™ EBT3 film measurements of dose enhancement effects by metallic nanoparticles for 192Ir brachytherapy, proton, photon and electron radiotherapy. Radiation. 2022;2(1):130-148.
39. Ahmad R, Royle G, Lourenço A, Schwarz M, Fracchiolla F, Ricketts K. Investigation into the effects of high-Z nanomaterials in proton therapy. Phys Med Biol. 2016 Jun;61(12):4537-4550.
40. Rashid RA, Abidin SZ, Anuar MA, Tominaga T, Akasaka H, Sasaki R, et al. Radiosensitization effects and ROS generation by high-Z metallic nanoparticles on human colon carcinoma cell (HCT116) irradiated under 150 MeV proton beam. OpenNano. 2019;4:100027.
41. Zwiehoff S, Johny J, Behrends C, Landmann A, Mentzel F, Bäumer C, et al. Enhancement of proton therapy efficiency by noble metal nanoparticles is driven by the number and chemical activity of surface atoms. Small. 2022 Mar;18(9).
42. Wang CC, Hsiao YY, Lee CC, Chao TC, Wang CC, Tung CJ. Monte Carlo simulations of therapeutic proton beams for relative biological effectiveness of double-strand break. Int J Radiat Biol. 2012 Jan;88(1-2):158-163.
43. Chaudhary P, Marshall TI, Currell FJ, Kacperek A, Schettino G, Prise KM, et al. Variations in the processing of DNA double-strand breaks along 60-MeV therapeutic proton beams. Int J Radiat Oncol Biol Phys. 2016 May;95(1):86-94.
44. Liu Y, Zhu K, Peng X, Luo S, Zhu J, Xiao W, et al. Proton relative biological effectiveness for the induction of DNA double strand breaks based on Geant4. Biomed Phys Eng Express. 2024 May;10(3):035015.